Measurement of Electrical Conductivity of Direct Digital Printed Conductive Traces Using Near-Field Microwave Microscopy

María F. Córdoba-Erazo, Eduardo A. Rojas-Nastrucci and Thomas. M. Weller
Center for Wireless and Microwave Information Systems, Department of Electrical Engineering, University of South Florida
Tampa, FL, 33620, USA
Email: maria15@mail.usf.edu, eduardor@mail.usf.edu, weller@usf.edu

Abstract
Non-contact measurement of electrical conductivity of direct digital manufactured traces using a dielectric resonator-based near-field microwave microscope (NFMM) operating at 5.73 GHz is reported. The NFMM uses a set of printed samples with known conductivity to build a calibration data set which correlates measured quality factor (Q) data with electrical conductivity (σ). Direct print additive manufacturing is used to produce the 10 mm x 10 mm calibration samples using CB028 silver ink and glass as the substrate. Conductivity of calibration samples ranges from 1.70e6 S/m to 3.22e6 S/m and it is measured using a commercially available four-point probe. Conductivity measurement of the calibration samples using NFMM reveals that the microscope is sensitive to printed samples with different conductivities and that it is able to resolve differences in conductivities as small as 0.38e6 S/m in the range 2.20e6 S/m ≤ σ ≤2.53e6 S/m. Conductivity and topography images of a printed trace are acquired simultaneously over a scan area of 100 μm x 100 μm using the non-contact NFMM at a distance of 3 μm from the sample. Conductivity images reveal that the conductivity is not constant over the scan area and that it varies from 0.6 S/m to 2 S/m. Roughness calculated from NFMM topography shows good agreement with the values computed from profilometer data.

Key words
Direct print additive manufacturing, electrical conductivity, imaging, non-contact scanning microwave microscopy, topography, printed electronics.

I. Introduction
Conductive inks are key materials that are being used in Direct Digital Manufacturing (DDM) for the fabrication of circuits and devices. The implementation of Ag thick film conductive ink has been reported for more than 30 years [1]. One of the advantages that this material offers is that it can be easily printed over a 3D surface while requiring a relatively low curing temperature (160° C for CB028) [2]. Previous works [3-5] characterized the curing process, electrical and surface properties of the material, using the conductivity calculated using DC measurements such as four-point probe, serpentine pattern, or Van der Paw technique. The use of this material in the realization of antennas [6], and more recently in the fabrication of microwave circuits [7]-[8] show the need of a characterization method at RF frequencies which provides localized material properties, rather than a averaged value. Typical techniques used to measure electrical conductivity of printed traces provide an averaged value of the electrical resistivity and do not show localized variations of the resistivity over the sample's surface, which can affect the performance of the printed structures, particularly for high frequency applications.

The fact that DDM technology generates highly rough surfaces and the sintering process of the ink results in an inhomogeneous particle distribution in the micron scale, escalates the importance of a measurement that provides conductivity with high spatial resolution, while at the same time resolving the surface relief.

NFMM is a non-contact, non-destructive technique used to measure the electromagnetic properties of materials such as dielectric constant, electrical conductivity and permeability on length scales shorter than the wavelength at the operation frequency [9]. The near-field term refers to the type of field interaction between the sensing probe of the microscope and the material under test (MUT). In a sensing probe terminated in a sharp tip whose diameter ϕ is much smaller than λ, as the one used in this work, the fields at the

end of the conductive tip are evanescent and they store electric or magnetic energy in the near-field of the tip, rather than carrying energy as traveling waves do in the far-field. Evanescent fields decay exponentially with distance, on a length scale on the order of ϕ. When a MUT is brought in close proximity to the tip, at a distance **d** usually less than ϕ, the charges on the tip are redistributed and the reactive fields around the tip are perturbed. This field perturbation is translated into changes in the resonant frequency Fr and Q of the resonator. Changes in the resonant properties of the probe can be correlated with the material properties by calibrating the NFMM using samples with known material properties [10-12]. Theoretical models based on cavity perturbation theory have also been used to correlate the shift in frequency to the dielectric constant of the insulating bulk samples and thin films [13],[14].

NFMM has been successfully used to image the sheet resistance R_s and the electrical resistance of direct digital printed resistors [15],[16]. In these works, the resistivity of the DuPont 7082 carbon ink was assumed to be constant across the samples; and the electrical resistance and *Rs* were found through Q measurements and a polynomial equation relating Q and the tip-sample distance **d**.

In this work, we measure the localized electrical conductivity of several conductive printed traces using a non-contact NFMM operating at 5.73 GHz. The conductive traces are made using CB028 silver ink, and a micro-dispense pump system. Additionally, we simultaneously acquire topography and electrical conductivity of a sample over an area of 100 µm x 100 µm. The electrical conductivity was found to vary between 0.6e6 S/m to 2e6 S/m.

II. Materials and Methods

A. Calibration samples

In order to measure the electrical conductivity using the NFMM, calibration samples were fabricated using additive digital printing manufacturing. They consisted of squares of size 10 mm x 10 mm, with thicknesses that are in the range of 25 µm to 65 µm. Glass 1 mm thick is used as the substrate since it provides a good surface for printing. The Ag microparticle CB028 ink [2] is used for the realization of the conductive layer. This ink was selected due to its good adhesion properties and ease of printing. Its curing process and other aspects such as particle size and adhesion have been previously characterized in [3] and [17] . Printing was performed using an nScrypt Tabletop microdispensing system. The printer setup consists of a Cartesian robot equipped with a SmartPump™ that dispenses a controllable low flow of ink (approximately 1.2 pL/s). The printing speed was in the range of 20-45 mm/s depending on the targeted thickness. The pressure of the system was constant at 15 psi, and the inner diameter of the pump tip is 125 um. The printing height was kept constant at 70 um during the printing process. After printing the ink is cured at 160° C for 1 h, as suggested in [2].

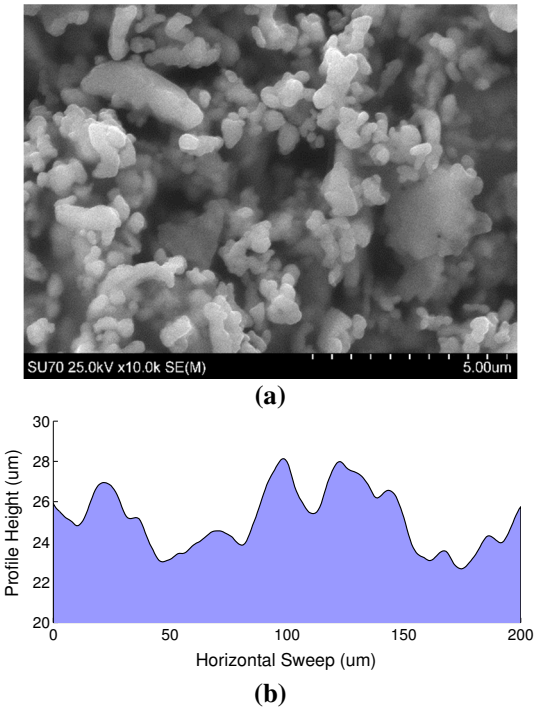

Fig. 1. Properties of the cured silver ink. (a) SEM image of the surface of a 25.2 um (average) thick sample. (b) Segment of profile of the same sample.

A SEM image over an area of 12 µm x12 µm of the surface of the ink after the curing process is shown in Fig. 1 (a). The SEM image was acquired using a Hitachi SU-70. The particle size of the ink after the curing process ranged between 0.5 µm to 4µm, with an average size of 2 µm, in agreement with [3]. A 200 µm profile across the sample was also measured using a Veeco Dektak 150 profilometer and is shown in Fig. 1 (b). This measurement is used for roughness calculation in the next sections.

B. DC-characterization

The conductivity value of the samples used for the calibration of the NFMM is obtained using the four-point probe method. The measurement is made with 1 mm probe spacing connected to a Jandel RM3000 meter. The resistivity of the sample is calculated using the equations for a thin rectangular slice [18]:

$$\rho = \frac{\pi}{Ln(2)} \cdot d \cdot CF \cdot \frac{V}{I} \qquad (1)$$

The resistivity (ρ) is function of the thickness (d) of the sample, and the ratio between the measured voltage (V) and current (I). The correction factor (CF) is used due to the

limited size of the sample (10 mm x 10 mm) compared to the probe spacing.

C. NFMM setup

A photograph of the NFMM used in this work is shown in Figure 2. It consists of an 8753 vector network analyzer (VNA) which is used as microwave source and detection system, a dielectric resonator (DR) -based microwave probe and a XYZ positioning system. The DR-based microwave probe operates at 5.73 GHz and consists of a dielectric resonator mounted on a RO4350B substrate and magnetically coupled to two 50 Ω microstrip lines as shown in Fig. 3 [19]. A commercially available gold-coated tungsten tip with radius of 25 µm is attached to a microstrip line 3λ/4 long. The resonant probe is enclosed in an aluminum cavity in order to prevent radiation and degradation of the resonator quality factor. The tungsten tip protrudes beyond one of the walls of the cavity through a hole with diameter of 5 mm.

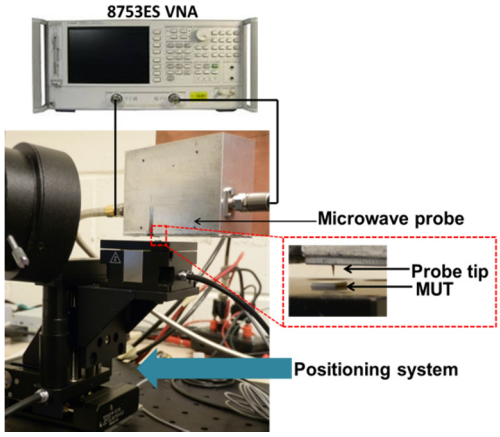

Fig.2. Photograph of the 5.73 GHz scanning near-field microwave microscope.

During scanning, the microwave probe is kept fixed while the MUT is positioned below the tip. In order to control the sample positioning, a computer-controlled scanning system was built. It consists of a XYZ-combination of Physik Instrumente M-112 1DG micro-translation stages for coarse motion and a Physik Instrumente P-611.Z piezo-stage for fine motion. The minimum incremental motion of the M112 1DG stage is 100 nm and the z-resolution for the P-611 Z piezo-stage is 2 nm. LabVIEW V.8.0 is used for the data acquisition and automation.

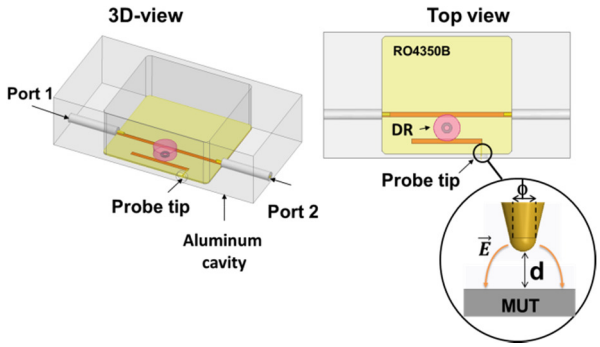

Fig.3. Schematic of the dielectric resonator (DR)-based near-field scanning microwave probe. The inset shows the tip geometry and MUT.

The evanescent fields at the end of the conductive probe tip are sensitive to the material properties of the MUT as well as the tip-sample distance **d**. Thus, the resonant properties of the microwave probe result affected by topography and material properties. To isolate these effects, a distance following feedback system must be integrated to the NFMM in order to perform scanning at constant tip-sample distance. Thus, NFMM allows one to perform simultaneous and independent imaging of both topography and conductivity of the MUT. Typical distance-following systems are complex and expensive. Examples of these systems are optical beam-bounce based feedback [20], tunneling current-based feedback [21], or tuning-fork-based feedback [22]. In this work, the use a low-cost and simple distance-following feedback mechanism which monitors the frequency shift that occurs at the contact point between the tip and the conductive sample. After the contact point has been stablished, the sample is lowered to the desired **d** and the resonant properties are recorded. Fig. 4 shows the measured S_{21} parameter of the microwave probe in air far from the sample (**d**=1000 µm), close to the sample (**d**=0.2 µm) and in contact with a conductive sample (**d**=0 µm). It can be seen that at the contact point the frequency shifts upwards by about 16 MHz compared to the position far from the sample.

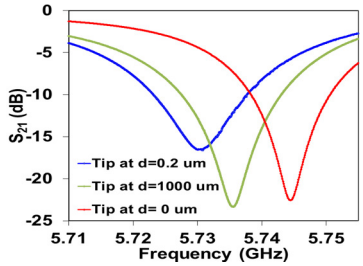

Fig.4. Measured S_{21} parameter of the microwave probe at d=0 µm (contact with the conductive sample) (red), d = 0.2 µm (blue) and d=1000 µm (green).

III. Results and Discussion

A. NFMM calibration and electrical conductivity extraction

The calibration of the NFMM is performed by recording Q as a function of **d** for the printed samples presented in Table I. This procedure was performed at four different points on the sample. The four points form a 300µm x 300µm square. Fig.5 shows the average of Q vs. **d** for each sample. From this figure, it can be seen that the NFMM is sensitive to samples with different conductivities (1.70e6 S/m ≤ σ ≤ 3.22 e6 S/m) and that the Q degrades as the conductivity of the sample decreases (thickness increases) and the tip-sample distance reduces. This behavior is explained by the fact that more energy is dissipated in samples with lower conductivities and this energy loss is more significant when the tip is close to the sample. The microscope is able to resolve differences in conductivity as small as 0.38e6 S/m in the range 2.20e6 S/m ≤ σ ≤ 2.58e6 S/m. Fig. 6 shows Q vs. conductivity of the calibration samples for d = 3 µm. The relationship between Q and the tip-sample distance can be approximated by a linear equation defined by σ = (Q-779.7)/53.7. The standard error in the mean was about ±7 for all samples. This high the error value is due to the significant roughness of the samples, found to be about R_q =1.5 µm over an area of 200 µm.

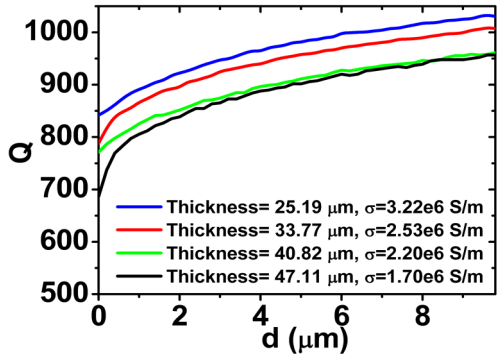

Fig.5. Q vs. d for calibration samples with different conductivities.

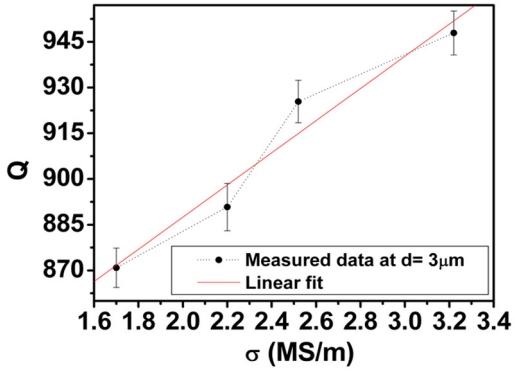

Fig.6. Q plot as a function of the electrical conductivity of printed traces at d= 3µm.

In order to test the method proposed, three additional samples were also printed on glass substrates using the same curing temperature and time employed for the calibration samples. For each sample, Q was measured at d=3 µm using the NFMM and the electrical conductivity was calculated using the linear equation previously presented. Thickness and electrical conductivity of the testing samples measured using NFMM are summarized in Table I. For comparison purposes, a third method of conductivity measurement is used. The expression proposed by Van der Pauw [23] is implemented to measure the conductivity of the 3 samples using the relationship:

$$e^{-\frac{\pi d}{\rho}R_{AB}} + e^{-\frac{\pi d}{\rho}R_{BC}} = 1 \qquad (2)$$

The four corners of the sample were named A, B, C, and D in a counterclockwise manner. R_{AB} represents the ratio of the voltage between corners A and B and the current applied through corners C and D. R_{BC} represents the ratio of the voltage $V_{BC}$and the applied current through corners A and D. The current for this measurement is set to 0.6 A. From (2), the value ρ is calculated, being known the d from the profilometer measurement.

Table I. Conductivity of testing samples measured using NFMM and the Van der Pauw technique

	Thickness (µm)	σ (S/m) using NFMM	σ (S/m) using Van der Pauw	Percentage difference
Sample 1	26.73	2.85e6	3.30e6	13.64
Sample 2	38.07	2.10e6	2.23e6	5.88
Sample 3	48.68	1.98e6	1.54e6	-28.73

Conductivity measurement using NFMM differs by less than ±29% compared to the Van der Pauw technique. This difference can be explained by the fact that NFMM provides a localized measurement of conductivity at microwave frequencies rather than a bulk measurement at DC. In NFMM, the volume under study in the sample is determined by the material properties, tip-size and tip-sample distance [9]. In order to determine this volume under study, a simulation of the electric fields around the tip and sample is carried out using the electrostatic simulator ANSYS Maxwell. The cross section of the sample in the simulator was recreated using a SEM image of a sample cured at 160°C for 1 hour as shown in Fig. 7 (a). Fig. 7(b) shows the tip-sample geometry used in simulations. The tip-sample distance is **d** = 3 µm. From Fig. 7 (c), the simulated electric fields around the tip and sample can be seen. In the sample, the fields decay by about half of the intensity in about 3 µm below the surface and vanish in about 6 µm. The fields extend laterally in the sample in a region about the diameter of the probe tip. Fields extension of about 6 µm in depth in this type of conductive sample is explained by fact that the material is composed of silver particles and air voids.

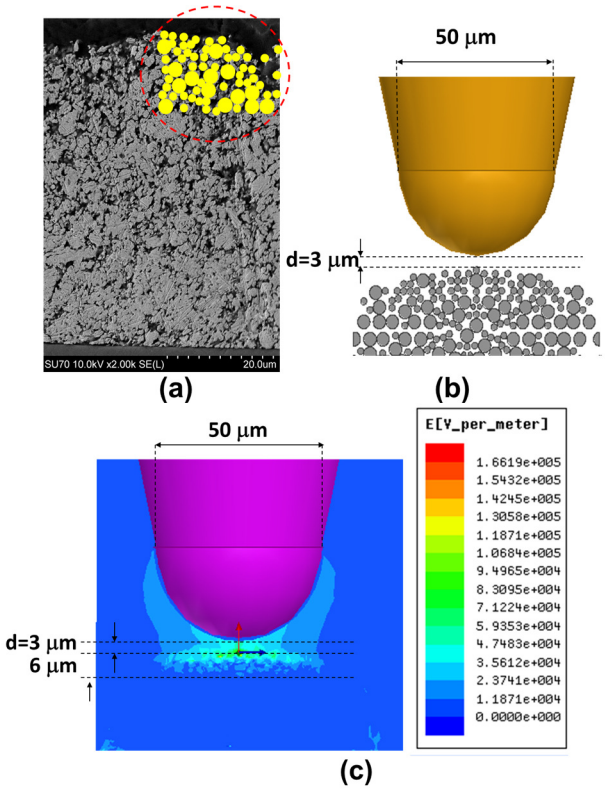

Fig.7. (a) SEM of the cross section of a sample cured at 160°C for one hour. In the region enclosed by the red circle, silver particles are represented by spheres with radius of 1 µm and 2 µm. This region was used as reference to recreate the sample in the electrostatic simulator. (b) Tip-sample geometry in ANSYS Maxwell. (c) Simulated E-field plots of the tip-sample interaction.

B. NFMM Imaging capability

The imaging capability of the NFMM was studied by scanning sample 1 of Table I over an area of 100 µm x 100 µm at a constant **d** = 3µm, in steps of 2 µm. At each point of the scan, Q and topography were simultaneously acquired. Then Q data were converted to electrical conductivity using the linear equation discussed in the previous sub-section. Fig. 8 (a) and (b) show the electrical conductivity and topography images obtained, respectively. The conductivity distribution in Fig. 8(a) indicates that the conductivity is not constant but varies between 0.6e6 S/m - 2e6S/m. Higher conductivity regions are observed over lower areas in the topography, which is in agreement with the observations in sub-section A, where higher conductivity was measured for thinner samples.

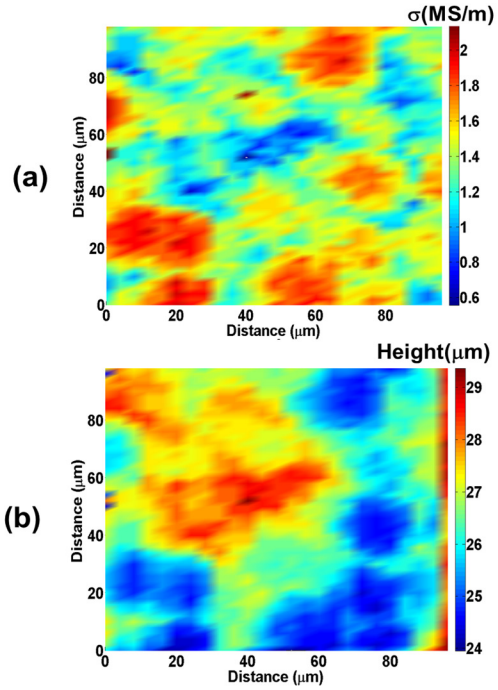

Fig.8. Conductivity and topography images over an area of 100 µm x100 µm obtained using the NFMM.

C. Statistical Analysis

The DC conductivity measurements of the samples showed that the overall conductivity decreases as the thickness increases. The reason of this behavior is still under investigation. A way to confirm this thickness-conductivity dependence using the NFMM is to compute the correlation between the topography and the conductivity images shown in Fig 8. The well-known expression for the correlation calculation is described in [24]:

$$\rho_{XY} = \frac{E\{(X-\mu_X)(Y-\mu_Y)\}}{\sigma_X \sigma_Y} \qquad (3)$$

Where ρ_{XY} is the correlation coefficient between X and Y variables, E is the expected value operator, μ represents the mean, and σ the standard deviation. In this work X is the conductivity and Y is the height value. The computed correlation coefficient between the two images is -0.7174. This implies that measured conductivity and topography are highly linearly inverse correlated; confirming the behavior of the resistivity obtained with the DC measurements

D. Surface Roughness

With the aim of validating the relief image obtained with the NFMM, the surface roughness of Fig.8 (b) is compared with the one obtained from the profile shown in Fig. 1(b). The parameters R_a (arithmetic average) and R_q (root mean squared) are calculated using (4) and (5). Z_i represents the height value for the i^{th} data point of the sample, n is the

total number of elements of the dataset, and μ_z is the mean value of the height.

$$R_a = \frac{1}{n}\sum_{i=1}^{n}|Z_i - \mu_z| \quad (4)$$

$$R_a = \sqrt{\frac{1}{n}\sum_{i=1}^{n}(Z_i - \mu_z)^2} \quad (5)$$

The dataset from the image covered a 100 µm x 100 µm area, and the one from the profilometer consisted of a 200 µm linear sweep. Although these calculations are comparing the height values of different regions of the same sample, there is a good agreement between the surface roughness parameters for the two measurement methods, as shown in Table II.

Table II. Surface Roughness comparison between the NFMM and profilometer data.

Roughness Coefficient / Data	Ra (um)	Rq (um)
Topography image (MFMM)	0.948	1.260
Linear Profile (Veeco Dektak 150)	1.128	1.487

IV. Conclusion

We have used a non-contact NFMM to image the electrical conductivity and topography of direct digital printed conductive traces, which were prepared using CB028 ink and a glass substrate. Conductivity images are acquired through Q measurements and a linear function that relates Q to electrical conductivity. Images revealed non-uniformity on the conductivity and a maximum variation of $\Delta\sigma$ = 1.4e6 S/m was observed over an area of 100 µm x 100 µm. Roughness computed from the topography extracted with the NFMM showed a good agreement with the value obtained from a profilometer measurement. The NFMM measurement was carried out at a constant height of 3 µm using a simple and novel mechanism, which detects the contact with the sample by sensing the resonance frequency of the NFMM probe. Advantages of using NFMM are that the conductivity measurement is performed in the microwave frequency regime, it is non-contact and non-destructive, and mapping of the electrical conductivity is possible. Moreover, the microwave probe along with the proximity sensor could be integrated with the printing tool in order to perform in-process characterization and quality control of printed devices. In this work, we are not claiming that NFMM is a replacement tool to the existing ones such as the four-point probe and Van der Pauw techniques but a complementary tool which can contribute to a better understanding of the localized electrical properties in the micron scale of additive manufactured samples in the microwave frequency regime.

Acknowledgment

This work was supported by the National Science Foundation Grant # ECS-0925968.

References

[1] W. Hicks, T. Allington, and V. Johnson, "Membrane Touch switches: Thick-Film Materials Systems and Processing Options," *Components, Hybrids, and Manufacturing Technology, IEEE Transactions on,* vol. 3, pp. 518-524, 1980.

[2] "DuPont CB028 Silver Conductor. Technical Data Sheet," DuPont, Ed., ed, 2013.

[3] D. A. Roberson, R. B. Wicker, L. E. Murr, K. Church, and E. MacDonald, "Microstructural and Process Characterization of Conductive Traces Printed from Ag Particulate Inks," *Materials,* vol. 4, pp. 963-979, 2011.

[4] A. Imtiaz, S. M. Anlage, J. D. Barry, and J. Melngailis, "Nanometer-scale material contrast imaging with a near-field microwave microscope," *Applied Physics Letters,* vol. 90, pp. 143106-143106-3, 2007.

[5] J. R. Greer and R. A. Street, "Thermal cure effects on electrical performance of nanoparticle silver inks," *Acta Materialia,* vol. 55, pp. 6345-6349, 10// 2007.

[6] P. V. Nikitin, S. Lam, and K. V. S. Rao, "Low cost silver ink RFID tag antennas," in *Antennas and Propagation Society International Symposium, 2005 IEEE*, 2005, pp. 353-356 vol. 2B.

[7] E. A. Rojas-Nastrucci, T. M. Weller, A. Vera Lopez, F. Cai, and J. Papapolymerou, "A Study on 3D-Printed Coplanar Waveguide with Meshed and Finite Ground Planes," presented at the Wireless and Microwave Technology Conference (WAMICON), 2014 IEEE, 2014.

[8] J. M. O'Brien, E. Rojas, and T. M. Weller, "A Switched-Line Phase Shifter Fabricated with Additive Manufacturing," presented at the 67th International Symposium on Microelectronics, 2013.

[9] S. Anlage, V. Talanov, and A. Schwartz, "Principles of Near-Field Microwave Microscopy," in *Scanning Probe Microscopy*, S. Kalinin and A. Gruverman, Eds., ed: Springer New York, 2007, pp. 215-253.

[10] M. Tabib-Azar, D. P. Su, A. Pohar, S. R. LeClair, and G. Ponchak, "0.4 um spatial resolution with 1 GHz (λ=30cm) evanescent microwave probe," *Review of Scientific Instruments,* vol. 70, pp. 1725-1729, 1999.

[11] V. V. Talanov, A. Scherz, and A. R. Schwartz, "A Microfabricated Near-Field Scanned Microwave Probe for Noncontact Dielectric Constant Metrology of Low-k Films," in *Microwave Symposium Digest, 2006. IEEE MTT-S International*, 2006, pp. 1618-1621.

[12] V. V. Talanov, A. Scherz, R. L. Moreland, and A. R. Schwartz, "Noncontact dielectric constant metrology of low-k interconnect films using a near-field scanned microwave probe," *Applied Physics Letters,* vol. 88, pp. 192906-192906-3, 2006.

[13] C. Gao, B. Hu, P. Zhang, M. Huang, W. Liu, and I. Takeuchi, "Quantitative microwave evanescent microscopy of dielectric thin films using a recursive image charge approach," *Applied Physics Letters,* vol. 84, pp. 4647-4649, 2004.

[14] C. Gao and X. D. Xiang, "Quantitative microwave near-field microscopy of dielectric properties," *Review of Scientific Instruments,* vol. 69, pp. 3846-3851, 1998.

[15] M. F. Cordoba-Erazo and T. M. Weller, "Non-contact characterization of printed resistors," *47th International Symposium on Microelectronics,* October 2013.

[16] M. F. Cordoba-Erazo and T. M. Weller, "Non-Contact Electrical Characterization of Printed Resistors using Microwave Microscopy," *IEEE Transactions on Instrumentation and Measurements*. Accepted for publication.

[17] S. Merilampi, T. Laine-Ma, and P. Ruuskanen, "The characterization of electrically conductive silver ink patterns on flexible substrates," *Microelectronics Reliability,* vol. 49, pp. 782-790, 7// 2009.

[18] "Geometric Factors in Four Point Resistivity Masurement," Haldor Topsoe, Semiconductor Division1966.

[19] M. F. Cordoba-Erazo and T. M. Weller, "Liquids characterization using a dielectric resonator-based microwave probe," in *42nd European Microwave Conference (EuMC),* 2012, pp. 655-658.

[20] M. Tabib-Azar and W. Yaqiang, "Design and fabrication of scanning near-field microwave probes compatible with atomic force microscopy to image embedded nanostructures," *Microwave Theory and Techniques, IEEE Transactions on,* vol. 52, pp. 971-979, 2004.

[21] A. Imtiaz and S. M. Anlage, "Effect of tip geometry on contrast and spatial resolution of the near-field microwave microscope," *Journal of Applied Physics,* vol. 100, pp. 044304-044304-8, 2006.

[22] J. C. Weber, J. B. Schlager, N. A. Sanford, A. Imtiaz, T. M. Wallis, L. M. Mansfield*, et al.*, "A near-field scanning microwave microscope for characterization of inhomogeneous photovoltaics," *Review of Scientific Instruments,* vol. 83, pp. 083702-083702-7, 2012.

[23] L. J. v. d. PAUW, "A Method of Measuring the Resistivity and Hall Coefficient on Lamellae of Arbitrary Shape," Phillips Technical Review1959.

[24] A. Snider, *Random Processes: A Companion Guide*, 2012.